Available online at www.sciencedirect.com
SCIENCE DIRECT®
International Journal of Heat and Fluid Flow 25 (2004) 593–605
International Journal of HEAT AND FLUID FLOW
www.elsevier.com/locate/ijhff

Numerical study of the instability mechanism in transitional separating–reattaching flow

Ibrahim E. Abdalla, Zhiyin Yang *

Department of Aeronautical and Automotive Engineering, Loughborough University, Loughborough LE11 3TU, UK

Received 9 July 2003; accepted 17 January 2004
Available online 9 April 2004

Abstract

Laminar separated flows are known to become unstable at relatively low Reynolds numbers. As a result, both the mean and instantaneous flow patterns are highly influenced by instabilities leading to transition to turbulence. Large-Eddy Simulation (LES) is employed to investigate the primary and secondary instabilities of a separated boundary layer transition on a flat plate with a blunt leading edge. The Reynolds number based on the uniform inlet velocity and the plate thickness is 6500. A dynamic subgrid-scale model is employed to compute the subgrid-scale stresses more accurately in the transitional flow case. Statistics of the LES are found to be in acceptable agreement with the available experimental data. Based on the characteristic frequency from the velocity and pressure spectra, the LES results confirm that transition starts with the primary 2D instability originating from the free shear in the bubble as the free shear layer is inviscidly unstable via the Kelvin–Helmholtz mechanism. The flow visualisation together with the spectral analysis for the velocity components and pressure give strong indication of the dominance of the *helical-pairing* instability which could be mainly responsible for the breakdown to turbulence.

Keywords: Large-eddy simulation; Separated boundary layer transition; Instability

1. Introduction

Laminar-turbulent transition is an important feature in aerospace aerodynamics and many other engineering flows. Despite many years of research on the fundamental mechanisms of the transition process in many generic configurations there are still many situations where they are not well understood and difficult to predict. The classical description of the transition from laminar flow to turbulence involves a sequence of primary stability, secondary stability,..., bifurcations which successively break the symmetries of the original problem (Manneville, 1990).

A free shear layer is formed as a laminar boundary layer separates from the edge of the blunt plate in the current study. Using conditionally averaged velocity vectors and contour lines of high-frequency turbulent energy Kiya and Sasaki (1985) visualised the three-dimensional features of the large-scale vortices in the reattaching zone of a separated flow on a blunt plate geometry like the case under study. They indicated that these large-scale vortices originated from a successive amalgamation of vortices formed in the separated shear layer owing to the *Kelvin–Holmholtz* instability. However, sufficient and detailed evidence has not been given in separated boundary layer transition studies to show that the instability mechanism at work is indeed the *Kelvin–Holmholtz* instability. Kiya and Sasaki's (1985) experiment showed that the large-scale vortices in the reattaching zone have a hairpin shape and that the spanwise distance between the ends of such vortices is approximately $0.6x_R$.

There are some similarities between plain mixing layers and the flow in the present study. For more reviews, the reader should refer to the papers by Cherry et al. (1984) for a blunt plate geometry, Srba (1996) and Pronchick and Kline (1983) regarding a backward-facing step geometry. The separated shear layer on a blunt plate can be considered as a mixing layer modified by a

* Corresponding author. Tel.: +05109227231.
E-mail addresses: i.e.abdalla@lboro.ac.uk (I.E. Abdalla), z.yang@lboro.ac.uk (Z. Yang).

0142-727X/$ - see front matter © 2004 Elsevier Inc. All rights reserved.
doi:10.1016/j.ijheatfluidflow.2004.01.004

Nomenclature

D	plate thickness
f_{max}	maximum frequency
h	shear layer thickness
K	wave number
K_{max}	maximum wave number
k_x	streamwise wave number
k_z	spanwise wave number
St	Strouhal number
$\overline{U}$	mean streamwise velocity
U_0	free-stream velocity
u_{rms}	root mean square value of the streamwise velocity
v_{rms}	root mean square value of the wall-normal velocity
x	streamwise axis
x^+	dimensionless distance along the streamwise axis
x_R	mean reattachment length of the separation bubble
y	wall-normal axis
y^+	dimensionless distance from the wall
y_c	shear layer center, and location of inflectional point
y_δ	edge of the shear layer
z	spanwise axis
z^+	dimensionless distance along the spanwise axis
Δx^+	streamwise mesh size in wall units
Δy^+	wall-normal mesh size in wall units
Δz^+	spanwise mesh size in wall units
ψ	stream function
ρ	density
τ_w	wall-shear stress
ν	molecular viscosity
ν_s	subgrid eddy viscosity

recirculation zone beneath it with a very unsteady reattachment region. Many aspects of similarity of the flow structures visualised in this study were found to be associated with those present in the case of plain mixing layers and the backward-facing step.

In the mixing layer experiment of Winant and Browand (1974) they noticed that the mixing layer is dominated by the presence of a quasi-two-dimensional spanwise vortical structures. They reported that neighbouring pairs of vortices roll around each other some distance downstream. The viscous diffusion smears out the identities of individual vortices to form a single large vortex from originally two vortices, a process they named *vortex pairing* which they believed to be the mechanism leading to transition in mixing layers. In other words, *vortex pairing* is a two-dimensional interaction whereby neighbouring vortices amalgamate to form a large vortex. Winant and Browand (1974) noticed that a considerable increase in smaller scale fluctuations is seen to occur at about the time of the second pairing but the large structure remains aligned across the stream, appearing two-dimensional in the mean. Chandrsuda et al. (1978) have directly observed generation of spanwise phase dislocation via localised pairing leading to vortices winding up around each other at the tip of the zigzags, yielding a quasi spanwise *double helix* vortex structure and gave the process the name *helical pairing*.

Other experiments have shown that the two-dimensional structures are subjected to three-dimensional instabilities (Miksad, 1972; Breidenthal, 1980; Bernal et al., 1981; Browand and Trout, 1980). Pierrehumbert and Widnal (1982) studied the two and three-dimensional instabilities of a spatially periodic shear layer by numerically solving the N-S equations. Their model consists of a family of coherent shear layer vortices discovered by Stuart (1967). From their simulation, Pierrehumbert and Widnal (1982) identified three types of secondary instability: the *helical pairing*, most unstable for 2D modes; *translative* instability which preserves the periodicity of the Stuart row and corresponds to the elliptic instability (Pierrehumbert, 1986) at large spanwise wave numbers and the so-called zigzag instability (Browan and Roshko, 1974) at short spanwise wave numbers; and finally a *core* instability associated with a varicose modulation of the core of the vortices. The three-dimensional instabilities are involved in the generation of small-scale erratic flow (Miksad, 1972; Bernal et al., 1981) but do not destroy the large-scale coherent structures (Browand and Trout, 1980). The vortex interactions thus play a role in the important stage of transition to three-dimensionality and indeed continue to influence characteristics of the developed turbulence downstream.

It is reasonable to assume that large structures in a given flow owe their origin to instabilities specific to that flow. Although there is no formal proof of this assumption the accumulated results from experiments for different flow fields do justify this assumption. In the experimental work of Bandyopadhyay (1991) in a backward-facing step geometry he argued that abrupt disintegration into smaller scales after pairing does not take place in low-disturbance mixing layers where the dominant large-structures are two-dimensional as reported by Winant and Browand (1974). He reported

that in spite of the many mixing-layer like characteristics of the backward-facing step flow there are some differences due to induced effects of the wall. Bandyopadhyay (1991) suspects that the disintegration is due to a three-dimensional instability of the two intertwining horseshoe vortices in the reattaching flow and that is why it succeeds the pairing instability. However, recently Delcayre (1997) has shown that helical pairing instability can transform the 2D *Kelvin–Helmholtz* rolls into Λ-shaped vortical structures, leading to three-dimensionality of the flow.

It is possible that many instability modes can exist and compete in the late stages of transition to turbulence. The mechanisms through which these instabilities work and destroy the 2D *Kelvin–Helmholtz* rolls are reasonably established for the case of mixing layers but seem to be far from fully understood for separated reattached flow. The secondary instabilities that occur in the case where the blunt plate extends up to the end of the domain in which the boundary layer separates at the leading edge, reattaches and develops into a turbulent boundary layer have received little analysis. The main objectives of this paper are: (a) to demonstrate that the free shear layer in the separation bubble is inviscidly unstable via the *Kelvin–Holmholtz* instability mechanism by analysing the LES data and comparing the results with those of the inviscid linear stability analysis; (b) to address the secondary instability leading to three-dimensionality of the flow and the associated flow structures.

2. Details of numerical computation

The governing equations are discretised on a staggered grid using the finite volume method. Any small-scale (smaller than the control volume) motions are averaged out and have to be accounted for by a subgrid-scale model. A standard dynamic subgrid-scale model in Cartesian co-ordinates has been employed in the present study. The ratio v_s/v is zero in the laminar region before transition occurs and starts to increase at about $x/x_R = 0.25$ reaching a maximum value of about 10 around the mean reattachment location and dropping down to about 5 after reattachment. The explicit second order Adams–Bashforth scheme is used for the momentum advancement. The Poisson equation for pressure is solved using an efficient hybrid Fourier multigrid method. The spatial discretisation is second-order central differencing which is widely used in LES owing to its non-dissipative and conservative properties. More details of the mathematical formulation and numerical methods have been reported elsewhere by Yang and Voke (2000).

The size of the computational domain is $25D \times 16D \times 4D$ along the x-, y- and z-axis respectively where $D = 10.0$ mm is the plate thickness. The origin of the x-coordinate is located $\frac{1}{2}D$ from the leading edge of the plate and the inflow boundary is at $x = -4.5D$ while the outflow boundary is at $x = 20.5D$. The lateral boundaries are at $8D$ from the surface, corresponding to a blockage ratio of 16. Two simulations were performed. In the first simulation $256 \times 164 \times 64$ cells along the streamwise, wall-normal and spanwise directions were used. In terms of wall units based on the frictional velocity downstream of reattachment at $x/x_R = 2.5$ the streamwise mesh sizes vary from $\Delta x^+ = 11.98$ to $\Delta x^+ = 59.92$, $\Delta z^+ = 24.96$ and at the wall $\Delta y^+ = 11.98$. The time step used in this simulation is $0.005655D/U_0$. The simulation ran for 65,000 time steps to allow the transition and turbulent boundary layer to become established, i.e., the flow has reached a statistically stationary state, and the averaged results were gathered over a further 312,000 steps with a sample taken every 10 time steps (31,200 samples) and averaged over the spanwise direction too, corresponding to around 63 flow-through or residence times.

In the second simulation the domain dimensions and the mesh cells along the streamwise and spanwise directions are the same as in the first simulation. Along the wall-normal direction the mesh was refined by using 212 cells. In terms of wall units based on the frictional velocity downstream of reattachment at $x/x_R = 2.5$ the streamwise mesh sizes vary from $\Delta x^+ = 9.7$ to 48.5, $\Delta z^+ = 20.2$ and at the wall $\Delta y^+ = 2.1$. The time step used in this simulation is $0.001885D/U_0$. The simulation ran for 70,000 time steps to allow the transition and turbulent boundary layer to become established and the averaged results presented below are then gathered over a further 399,000 steps with a sample taken every 10 time steps (39,900 samples) and averaged over the spanwise direction too, corresponding to around 28 flow-through or residence times. Instantaneous flow fields and time traces of velocity components at certain points were also stored during the two simulations for the purpose of visualisation and analysis. Comparisons between the two sets of results in terms of flow structures and spectra show little difference, but the second set has better statistical agreement with the available experimental data.

A free-slip but impermeable boundary condition is applied on the lateral boundaries. In the spanwise direction, the flow is assumed to be statistically homogeneous and periodic boundary conditions are used. No-slip boundary conditions are used at all other walls. The uniform inflow velocity U_0 is 9.425 m/s and aligned with the plate. The Reynolds number based on the inflow velocity and plate thickness is 6500. On the outflow boundary, a convective boundary condition is applied.

In the present study the center of the shear layer (y_c) is defined as the y-location where the rms of the streamwise velocity (u_{rms}) attains a maximum value, consistent with the definition of Kiya and Sasaki (1983)

(hereafter referred to as KS). The edge of the shear layer, y_δ, is defined as the locus of points where $u_{\rm rms}/U_0$ has a value of 2.5%. This definition is consistent with the experimental studies of Djilali and Gartshore (1991) and Cherry et al. (1984).

3. Results and discussion

3.1. Mean flow variables

The mean position of reattachment is an important parameter characterising a separated/reattached flow. There are four methods to determine the mean reattachment location according to Hung et al. (1997) in their DNS study for backward-facing step flow. These methods are: (a) by the location at which the mean velocity $U = 0$ at the first grid point away from the wall; (b) by the location of zero wall-shear stress ($\tau_w = 0$, or $\partial U/\partial y = 0$); (c) by the location of the mean dividing streamline ($\psi = 0$); and (d) by a *p.d.f.* method in which the mean reattachment point is indicated by the location of 50% forward flow fraction. They found that the first three methods are within 0.1% of each other, and about 2% different from the *p.d.f* results. Therefore the first method was used to determine the mean reattachment length in the current study. Fig. 1 shows the mean streamwise velocity at the first grid point away from the wall along the x-axis. The figure shows that the location at which the mean velocity $U = 0$ is at $x/D = 6.0$. As the origin of the x-coordinate is located $\frac{1}{2}D$ from the leading edge of the plate, the reattachment length of the bubble is $6.5D$.

The current LES results will be compared with experimental data by Castro and Epik (1998) (hereafter referred to as CE) as the same geometry and Reynolds number used in the experiment by CE are used in the current study. However, it is worth pointing out that in the experiment CE (1998) used a flap to control the length of the bubble. In addition, the blockage ratio of the experiment is approximately four times that of the simulation which will certainly contribute to some of the discrepancies.

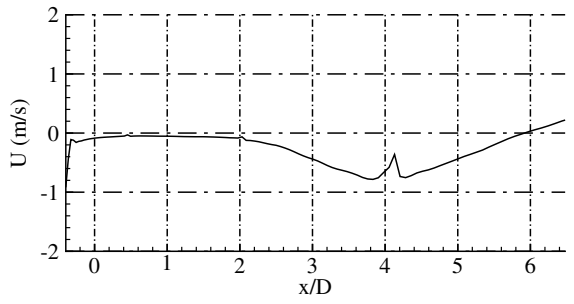

Fig. 1. Streamwise mean velocity profile at the first cell from the solid surface along the streamwise direction.

Due to the very limited data from CE (1998) the LES results are also compared with the experimental data by KS (1983) and the numerical results by Tafti and Vanka (1991) (hereafter referred to as TV). To facilitate comparison the profiles are plotted either as function of y/x_R or $(y - y_c)/x_R$ at corresponding values of x/x_R, where y_c is the center of the shear layer and x_R is the mean reattachment length. The measured bubble length is $7.7D$ by Castro and Epik (1998) which is bigger than the simulated bubble length (about $6.5D$). This is a reasonably good agreement taking into account the effect of flap and blockage ratio as mentioned above. Cherry et al. (1984) reported a value of $4.9D \pm 0.05D$ at a higher Reynolds number ($3.2\times10^4 \pm 0.2\times10^4$). They also reported that the bubble length started to increase when the Reynolds number was reduced below 3.0×10^4. They attributed this to the gradual extension of the laminar shear layer seen in the visualisation of Hillier and Cherry (1981). KS (1983) reported a slightly higher value of the mean reattachment length ($5.05D$) for a Reynolds number of 2.6×10^4 while TV (1991) predicted a value of $6.3D$ for a low Reynolds number (1000) case. It is likely that at higher Reynolds numbers transition occurs earlier or it could be turbulent separation leading to a shorter laminar part of the bubble which leads to a shorter bubble than that for the lower Reynolds number cases.

Another important difference between the current simulation and the literature cited above is the ratio of the spanwise dimension to the plate thickness (z/D). The ratio for the current study is 4 compared to 10 for KS (1983) and 13.2 for Cherry et al. (1984). It has been reported by Cherry et al. (1984) that the dependence of the mean reattachment length on the ratio is weak and therefore it is likely that Reynolds number plays a more important role.

Fig. 2 compares the mean streamwise velocity distribution $\overline{U}/U_0$ with the experimental data by KS (1983) and the numerical results of TV (1991) at three streamwise locations. The results show a reasonably good agreement with the data of KS (1983). The predicted peak and the free stream values of the velocity are bigger than those measured by KS (1983). This discrepancy is most likely due to the fact that it is laminar separation in the present study but turbulent separation in the experiment by KS (1983) and also the differences in blockage ratio as it is 20 in the experiment by KS (1983) and 16 in the current study. The results of TV (1991) have a better agreement with the current LES results compared with those of KS (1983). The possible explanation is that the Reynolds numbers are relatively low in both simulations and the blockage ratio is the same.

Profiles of the *rms* of streamwise velocity, $u_{\rm rms}$ normalised by U_0, at the same three stations are shown in Fig. 3. The agreement between the LES results and the

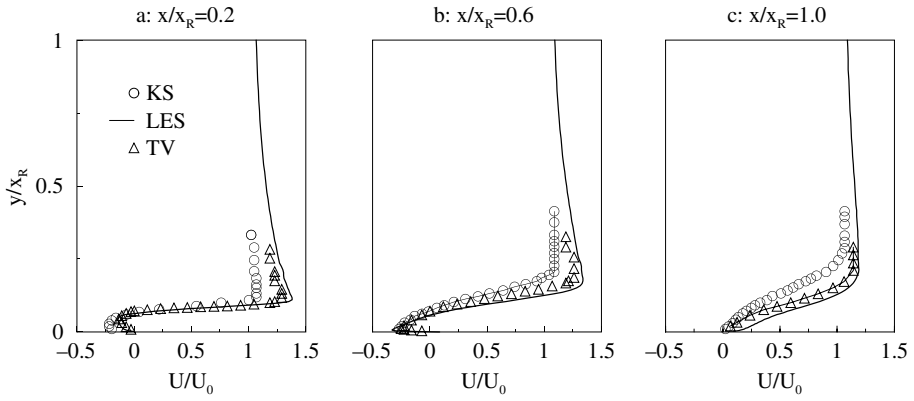

Fig. 2. Profiles of mean streamwise velocity $\overline{U}/U_0$ at three streamwise locations. Also shown are measurements by KS (1983) at $Re = 26,000$, and numerical results by TV (1991) at $Re = 1,000$.

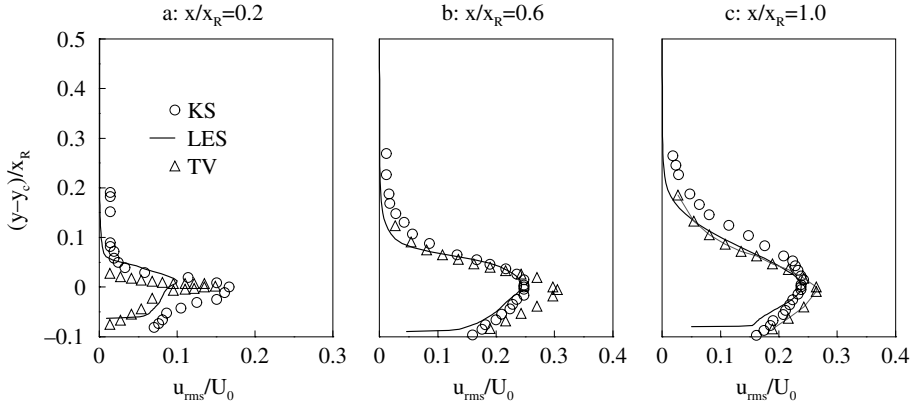

Fig. 3. Profiles of mean streamwise turbulent intensity $u_{\rm rms}/U_0$ at three streamwise locations. Also shown are measurements by KS (1983) at $Re = 26,000$, and numerical results by TV (1991) at $Re = 1,000$.

data of KS (1983) and results of TV (1991) is reasonably good taking into account the fact that the Reynolds numbers and blockage ratio are different as mentioned above, and that in the experiment it was turbulent separation whereas it is laminar separation in the present study. At the first location ($x/x_{\rm R} = 0.2$) where the currently predicted flow is still laminar the peak value of $u_{\rm rms}/U_0$ is smaller than those measured by KS (1983) and predicted by TV (1991). The current LES predicts a maximum value of $u_{\rm rms}$ of $0.285U_0$ at $x/x_{\rm R} = 0.8$. Simulation by TV (1991) shows a maximum value of order $u_{\rm rms}/U_0 = 0.32$ in the region $x/x_{\rm R} = 0.55 - 0.7$, while the measured maximum $u_{\rm rms}$ by KS (1983) is $0.26U_0$ at $x/x_{\rm R} = 0.8$. Other experimental studies (Djilali and Gartshore, 1991) have shown maximum $u_{\rm rms}$ of up to $0.3U_0$. Overall, the profiles of $u_{\rm rms}$ show a reasonably good agreement with the data.

The comparison of the Reynolds stresses at the mean reattachment location ($x/x_{\rm R} = 1.0$) with the data of KS (1983) and CE (1998) is shown in Fig. 4. It can be seen that the current LES overpredicts the maximum value for $u_{\rm rms}/U_0$ and $v_{\rm rms}/U_0$ when compared with the experimental data by CE (1998) at the same Reynolds number. Measurements by CE (1998) show a maximum value for $u_{\rm rms}/U_0$, $v_{\rm rms}/U_0$, and uv/U_0^2 of order 0.19, 0.13 and 0.014. The LES predictions are 0.25, 0.20 and 0.015 respectively while the data of KS (1983) suggest the corresponding values to be of order 0.25, 0.20 and 0.021. The LES results are in agreement with the KS (1983) data apart from the $-uv/U_0^2$ variable and have a better agreement with the data of CE (1998) as far as $-uv/U_0^2$ is concerned.

4. Primary instability mechanism

4.1. Position of initial unsteadiness

The flow is laminar and two-dimensional before the separation and just after the separation as can be seen from Fig. 5 which shows the instantaneous spanwise velocity at three arbitrary times in the spanwise plane $z/x_{\rm R} = 0.4$ along the streamwise direction starting from the separation point. It can be seen clearly that the

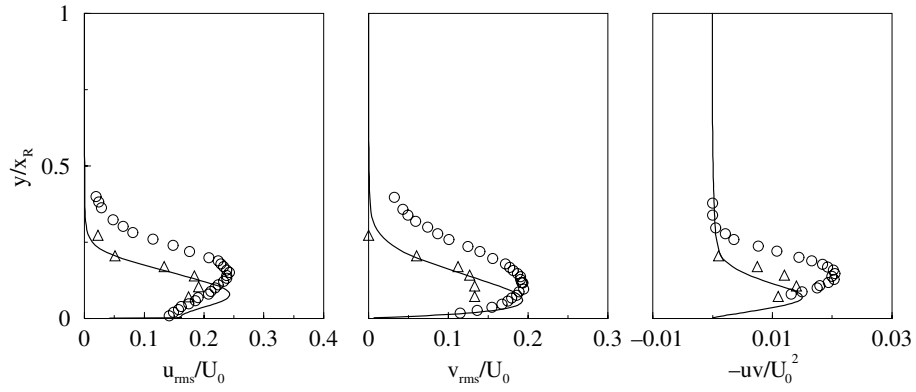

Fig. 4. Reynolds stresses at the mean reattachment location. Also shown are the measurement by KS (1983) at $Re = 26,000$ and the data of CE (1998) at the same location and same Reynolds number.

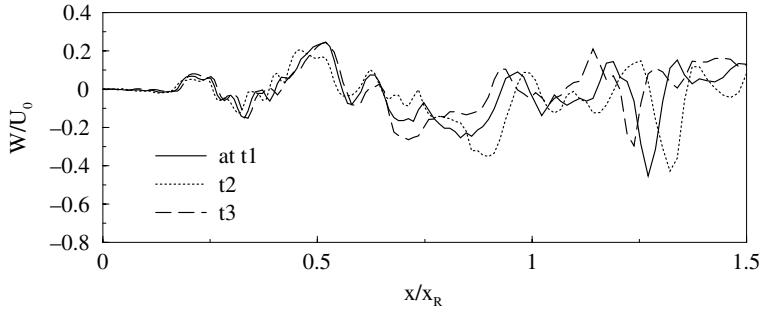

Fig. 5. Instantaneous spanwise velocity profiles at $y/x_R = 0.02$.

profiles at three different times are virtually the same up to $x/x_R \approx 0.225$, with the spanwise velocity W being zero indicating that the flow is two-dimensional and steady. The profiles indicate that the position of unsteadiness occurs at about $x/x_R \approx 0.225$. The instantaneous spanwise velocity starts to develop slowly when $x/x_R \geqslant 0.225$ and remains small until $x/x_R \approx 0.5$ when significant three-dimensional motion starts to develop very quickly and violently with maximum values reaching almost 42.5% of the streamwise velocity in the free stream.

The breakdown of the laminar shear layer is best viewed by Fig. 6 which shows the streamwise velocity contours at several streamwise location $x/x_R = 0.25$, 0.5 and 0.95. Initially, at $x/x_R = 0.25$, low amplitude waves can bee seen in the laminar shear layer, then the amplitude increases considerably at $x/x_R = 0.5$ but the structures remain fairly organised. Approaching reattachment, the structures appear to be irregular and the spanwise symmetry is totally broken at $x/x_R = 0.95$ within the reattachment region.

It is evident from the figures discussed above that the flow starts to become unsteady in the region from $x/x_R = 0.2$ to $x/x_R = 0.25$ and significant growth of the disturbances starts at about $x/x_R = 0.5$.

To clarify whether the instability of the free shear layer in the present study is the *Kelvin–Holmholtz* instability we will consider the *Kelvin–Holmholtz* instability mechanism in more detail for the case of two uniform incompressible inviscid fluids of densities ρ_1, ρ_2 and velocity U_1, U_2 separated by a horizontal boundary at $y = 0$. For any difference $U_1 - U_2$, no matter how small it is, instability occurs for all wave-numbers greater than a critical value. This is the *Kelvin–Helmholtz* instability as stated by Chandrasekhar (1961). To further clarify whether the independence of the *Kelvin–Helmholtz* instability on $|U1 - U2|$ is due to the sharp discontinuities in ρ and U which have been assumed in its derivation Chandrasekhar (1961) considered the case of continuous variation of U and a certain distribution of ρ (characterised by the Richardson number) and when the Richardson number is zero, i.e., for constant density, the condition for the *Kelvin–Helmholtz* instability is $0 < Kh < 1.2785$ where K is the wave number and h is the shear layer thickness. In the present study the shear layer thickness in the region where the unsteadiness first becomes apparent at about $x/x_r = 0.225$ is $0.0875x_R$ and hence the unstable region for K is $0 < K < 14.6/x_R$. In other words the *Kelvin–Helmholtz* instability will not occur in the present study for wave numbers higher than $14.6/x_R$, or wave lengths smaller than $2\pi/K = 0.4x_R$. Fig. 7 shows the spectra for the velocity components U, V, W and the pressure P at $x/x_R = 0.75$, $y/x_R = 0.13$. It is apparent from the spec-

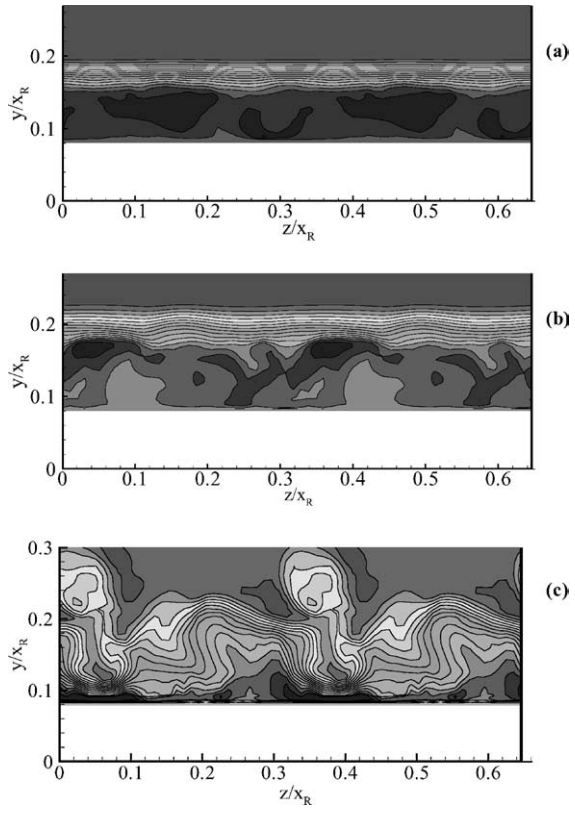

Fig. 6. Instantaneous streamwise velocity contours at (a) $x/x_R = 0.25$, (b) 0.5, and (c) 0.95.

tra that the characteristics frequency in the present study varies between $0.225 \leqslant St \leqslant 0.275$ equivalent to 126–158 Hz or $0.7 - 0.875U_0/x_R$. The wave speed c is equal to the velocity at the critical layer, $U(y_c)$, i.e., the streamwise velocity at the inflection point where $\frac{d^2U(y_c)}{dy^2} = 0.0$, which is about $0.428U_0$ at $x/x_R = 0.225$. Based on this the maximum wave number from the simulated results is $K_{max} = 2\pi f_{max}/c = 12.85/x_R$, corresponding to a wavelength of $0.489x_R$, which satisfies the *Kelvin–Helmholtz* instability criterion for the present study $(0 < K < 14.6/x_R)$. Thus it can be concluded that the free shear layer in the separation bubble is most likely to become inviscidly unstable via the *Kelvin–Helmholtz* instability mechanism. Similar calculation for the region up to $x/x_R = 0.45$ is done and the values appear in Table 1.

4.2. Flow structures and secondary instability

The flow structures have been visualised by three methods which are: low-pressure fluctuation isosurfaces, the Q-criteria, and vorticity modulus. The degree of clarity of structures shown by each method in the current study has been discussed elsewhere by Abdalla and Yang (in press). Visualisation through low-pressure fluctuation isosurfaces has been found to be better showing the flow structures before and after reattachment in comparison with the other two methods. Figs. 8–11 show pressure isosurfaces with $p' = -0.1\rho U_0^2$ apart from Fig. 9c which corresponds to $p' = -0.05\rho U_0^2$. The data for these figures were collected every 1000 time step after the simulation ran for 150,000 time steps (equivalent to $t = 283D/U_0$). The figures discussed below are selected from among the very extensive data collected in order to visualise the structures. It is worth pointing out that the evolution process of these structures start from the shedding of *Kelvin–Helmholtz* billows which undergo transformation into 3D structures in the reattachment region, breaking to small-scale turbulent structures after the reattachment. This cycle was noticed to take a period of about 10,000 time steps (equivalent to $t = 18.85D/U_0$) but the process is not really periodic in the sense that it repeats itself exactly after the above-mentioned period. The figures are selected to show the structures rather than their evolution in a single cycle which has been discussed elsewhere by Abdalla and Yang (in press).

At the onset of *Kelvin–Helmholtz* instability, *Kelvin–Helmholtz* billows are formed downstream of the plate leading edge and grow in size as they travel downstream. This is clearly demonstrated by Fig. 8a and b which show two spanwise vortex tubes (*rolls*). The *Kelvin–Helmholtz* rolls grow in size and are subjected to approximately sinusoidal undulation (waviness) along the spanwise. It can clearly be seen that the axis of the spanwise rolls remains perpendicular to the flow direction thus keeping their coherency and two-dimensionality nature up to this stage. The *Kelvin–Helmholtz* rolls in Fig. 8a and b also indicate that in addition to the spanwise waviness, peaks and valleys also start to develop. This is a characteristic of triggering due to large disturbances in this specific region where the 3D motion is developed as discussed previously. The spanwise waviness creates some topological changes in the *Kelvin–Helmholtz* rolls as shown in the second roll of the Fig. 8a and b, creating a zigzagging array of vortices. The same phenomenon is noticed in the first roll although not as apparent as in the second roll due to its distorted nature around the mean reattachment location.

Similar observations have been reported for related flows. The study of the mixing layer by Wygnanski et al.

Table 1

x/x_r	0.259	0.274	0.29	0.30	0.32	0.34	0.35	0.37	0.39	0.41	0.42	0.44
$K * x_R$	12.38	10.43	11.6	9.8	10.5	11.3	9.5	10.0	10.7	11.2	11.5	9.5

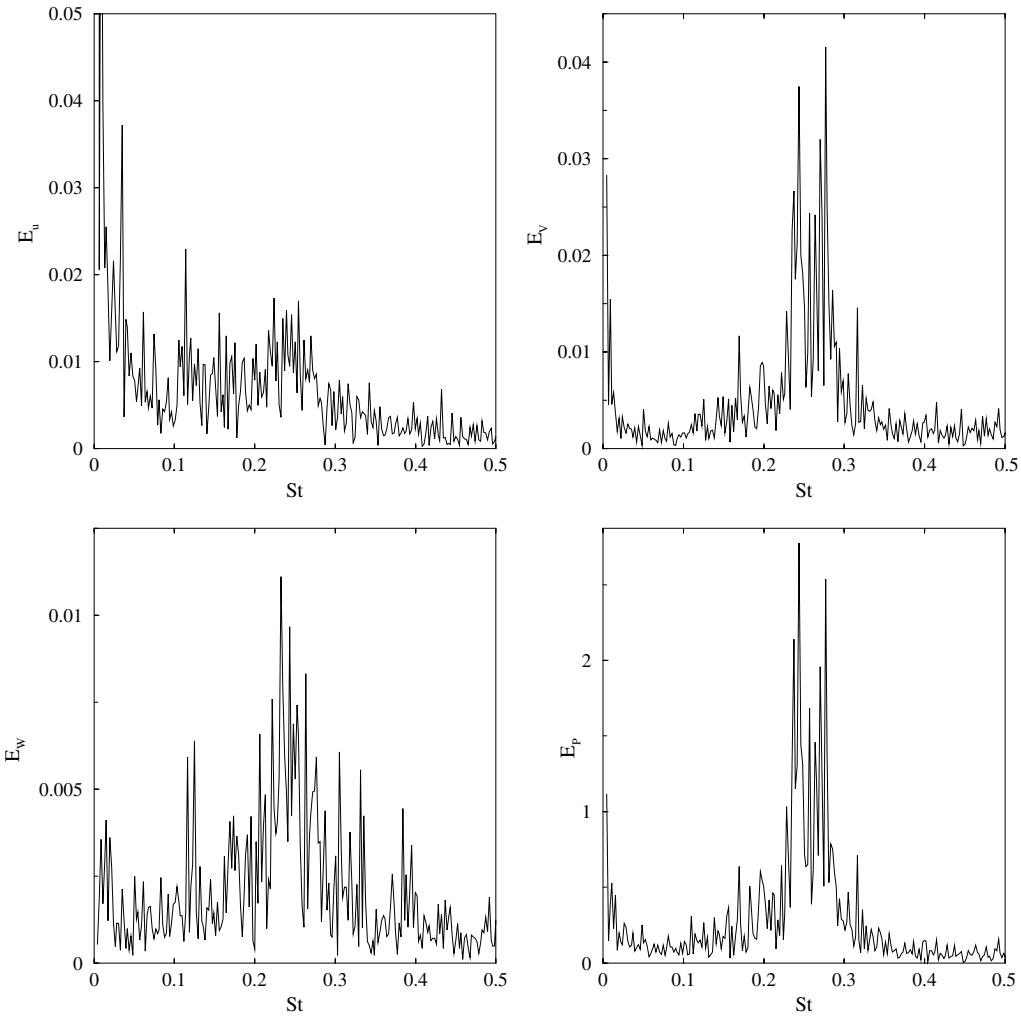

Fig. 7. Spectra for the velocity components U, V, W and the pressure P at $x/x_R = 0.75$, $y/x_R = 0.13$, $z/x_R = 0.2$.

(1979), Browand and Trout (1980), Breidenthal (1980), Roshko (1981), Oguchi and Inoue (1984), Lasheras and Choi (1988), Comte et al. (1992) and others have shown that even under the influence of strong external disturbances the mixing layer is dominated by the presence of a quasi-two-dimensional spanwise vortical structures. *Kelvin–Helmholtz* rolls were also noticed in the flow of a backward-facing step (Neto et al., 1993; Delcayre, 1997). This is an indication that similar mechanisms responsible for the breakdown of *Kelvin–Helmholtz* rolls into smaller scales in these studies could work here. It is evident from the present study that almost none of the 2D structures could survive the reattachment region. In the region between $x/x_R = 0.5$ and 1.0 such rolls are subjected to severe distortion which degrade their two-dimensionality completely.

The time evolution of modal energies (Comte et al., 1992) suggests that the flow topology observed at this stage can be interpreted as the result of oblique modes. For a shear flow perturbed by a transverse perturbation $v'(x,z)$ composed of a pair of unstable oblique waves of equal amplitudes

$$v' \propto [\cos(k_x x + k_z z) + \cos(k_x x - k_z z)] = 2\cos(k_x x)\cos(k_z z) \quad (1)$$

Loci where v' is extremal make a staggered array of streamwise period $2\pi/k_x$ and spanwise $2\pi/k_z$. The amplification of the waves will lift up vorticity where v' is positive (peaks) and bring down vorticity where v' is negative (valleys). The former will be, to the lowest order, advanced by the upper stream at a velocity $+U$, the latter by the lower stream at $-U$ yielding the zigzagging array of vortices. Numerical proof of this process was given by Sandham and Reynolds (1991) in the case of a compressible mixing layer forced initially by two equal and opposite oblique waves. In the present incompressible case it seems that the same process is at work.

Fig. 9b shows that the first roll consists of intertwining vortices forming a structure of helical nature.

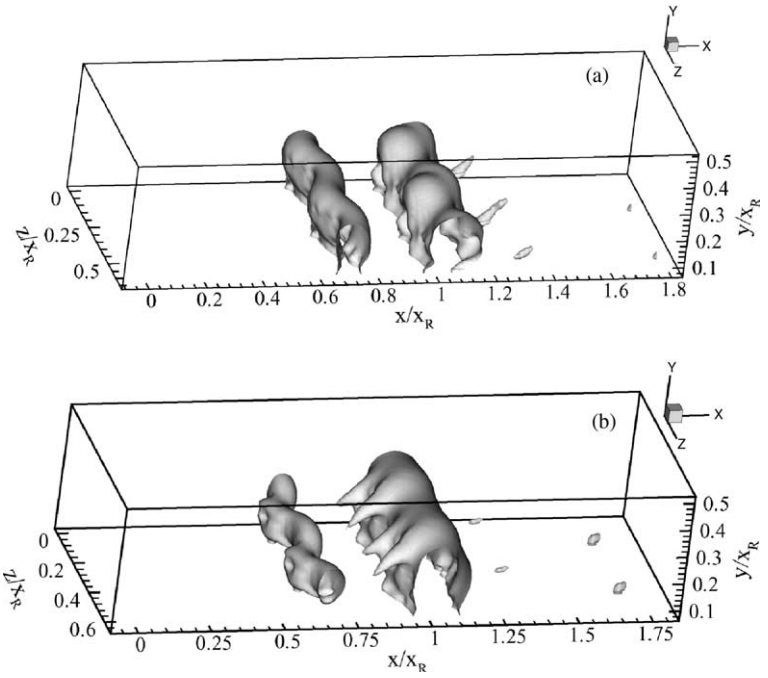

Fig. 8. Low-pressure isosurfaces displaying KH rolls subjected to spanwise waviness: (a) $t = 309.1D/U_0$; (b) $t = 361.9D/U_0$.

With a slightly lower pressure level Fig. 9c shows about three pairings which indicate that possibly the smooth *Kelvin–Helmholtz* rolls shown in Fig. 8a and b are sometimes resulting from pairing process in the sense described by Chandrsuda et al. (1978). The third roll in Fig. 9c is typical to what is noticed in Fig. 8.

From the above discussion it is clear that the structures shown by the flow visualisation clearly bear all the characteristics of the "helical-pairing instability". However, the flow visualisation did not really show two separate *Kelvin–Helmholtz* rolls merging together in a pairing process to form a double helix structure. For example Fig. 9b and c all give an indication that up to $x/x_R = 0.75$ the structures are most likely consisting of two *Kelvin–Helmholtz* rolls in the process of pairing but the view when they are approaching each other is captured only once as seen in Fig. 9a among the extensive data we analysed. It is possible that this process takes a very short period of time and was not captured in the current study as the data we are presenting here were taken at 1000 time steps apart.

Another important observation can be deduced from Fig. 8a and b by investigation of the topological changes between the two *Kelvin–Helmholtz* rolls along the streamwise direction. The three figures indicate that the instability mechanism displaces the adjacent rolls in opposite directions. In other words the oscillation of two adjacent *Kelvin–Helmholtz* rolls is not in-phase. Generally speaking, the subharmonic modes are modes in which adjacent vortices are displaced in opposite directions. This is a another indication of the fact that the instability involved is most likely the helical-pairing instability which belongs to the subharmonic family.

The flow visualisation shows that while travelling downstream the above described 2D spanwise coherent vortical structures become more distorted (specially the initially shed roll) leading to the appearance of a well-organised array of streamwise vortices originating from the initially shed vortical tube. Fig. 10a and b reveal that *Kelvin–Helmholtz* billows have been transformed into Λ-shaped vortices while Fig. 11a and b display the transformation of the *Kelvin–Helmholtz* billows into longitudinal streamwise vortical structures popularly known as *ribs*. Fig. 12 shows the velocity vectors (v, w) on the (y, z) plane at the streamwise location $x/x_R = 0.8$. The figure clearly indicates the existence of the counter-rotating vortices as an evidence of the Λ-shaped vortices. The spanwise distance between the ends of the hairpin vortices shown in Fig. 10a and b is approximately $0.3 - 0.33x_R$, which is roughly the same as the *Kelvin–Helmholtz* wavelength in the present study. This is worthy of note as it is shown by Roshko (1981) that the spanwise distance between the streamwise vortices in the transition region of an initially laminar mixing layer is approximately equal to the *Kelvin–Helmholtz* spacing. In the LES simulation of a transitional separated boundary-layer due to surface curvature, Yang and Voke (2001) estimated the spanwise distance between the ends of the hairpin vortices as 0.31 while Kiya and Sasaki's (1985) experiment showed that this distance is approximately $0.6x_R$. It is not clear from the present study why there is such a discrepancy despite that the

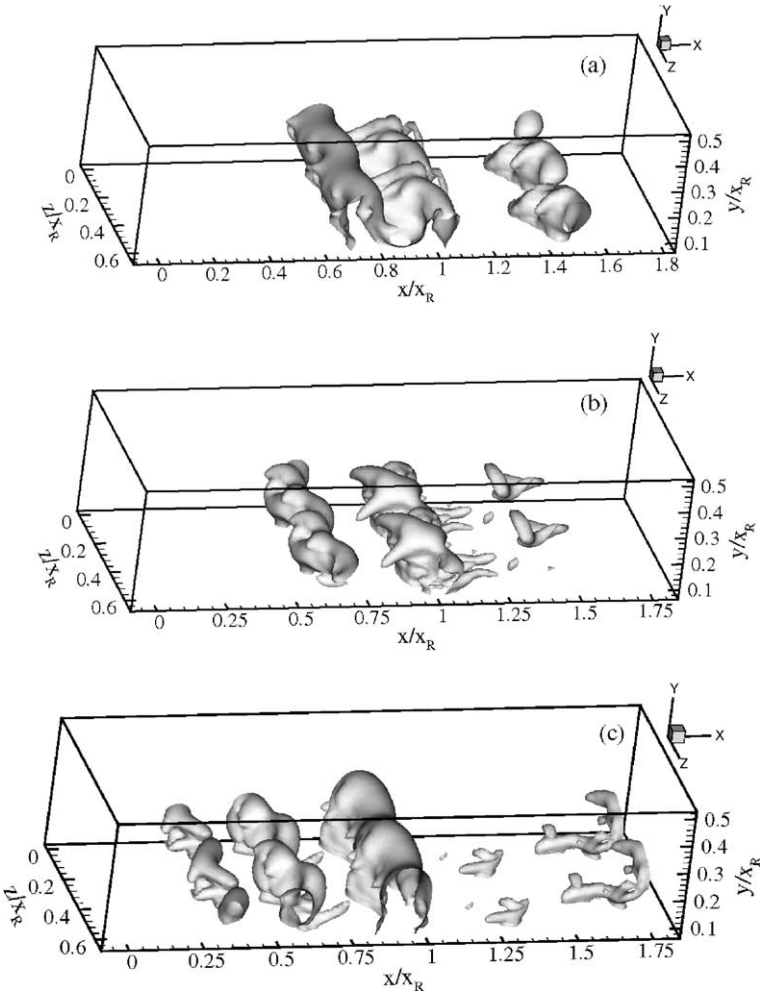

Fig. 9. Low-pressure isosurfaces displaying how pairing process can take place in the current study: (a) $t = 322.3D/U_0$; (b) $t = 390.2D/U_0$; (c) $t = 452.4D/U_0$.

spanwise dimension (z/D) is different in the experiment ($z/D = 10$) and the simulations ($z/D = 4$ in the current study and $z/D = 2$ in the simulation by Yang and Voke (2001)). However, we do not think the spanwise dimension is the major reason behind this and further study is needed.

In translative instability everything would oscillate in-phase including the structures. Moreover, experiments (Bernal et al., 1981) indicate that the translative instability leads to the generation of small-scale turbulence and increased mixedness but leaves the large-scale structure relatively intact. Flow visualisation in the current study does not give any indication of the existence of this type of instability at any part of the flow. This is because in the first instance the three-dimensional coherent structures (Λ-shaped and Ribs) evolve as topological consequences from the distorted *Kelvin–Helmholtz* rolls. In addition, as discussed above, the rolls do not oscillate exactly in-phase. Hence the topological changes revealed by the flow visualisation do not exhibit the characteristics of translative instability.

Thus, from the above discussion, it is plausible that the transformation of the *Kelvin–Helmholtz* rolls into three-dimensional structures (Λ-shaped and Ribs) is likely to be due to the helical pairing instability in the present study. The pairing and the hairpin (Λ-shaped) vortices play an important role in the transition process towards three-dimensionality in the current study. Indeed, the hairpin vortices become part of the core of the spanwise vortex resulting from the pairing instability that distorts and breaks the *Kelvin–Helmholtz* rolls into 3D coherent vortices. It is reasonable to assume that the way the streamwise evolving vortices interact with the spanwise vortices is by aligning more vorticity from the spanwise into the streamwise vortices thus making them to grow and become larger while degrading the coherency of the spanwise vortical rolls.

The pressure and velocity spectra in Fig. 7 shed more light on the origin of the instability involved here. The location $x/x_R = 0.75$ is selected because it corresponds to an intermediate location between $0.5 \leqslant x/x_R \leqslant 1.0$ within which the flow visualisations have shown that

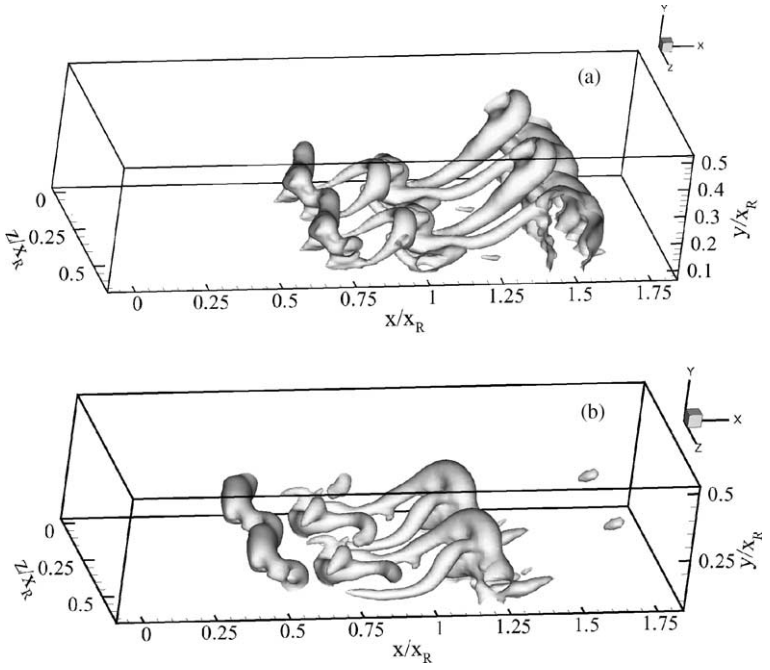

Fig. 10. Low-pressure isosurfaces displaying how *Kelvin–Helmholtz* rolls have been transformed into Λ-shaped vortices: (a) $t = 299.7D/U_0$; (b) $t = 348.7D/U_0$.

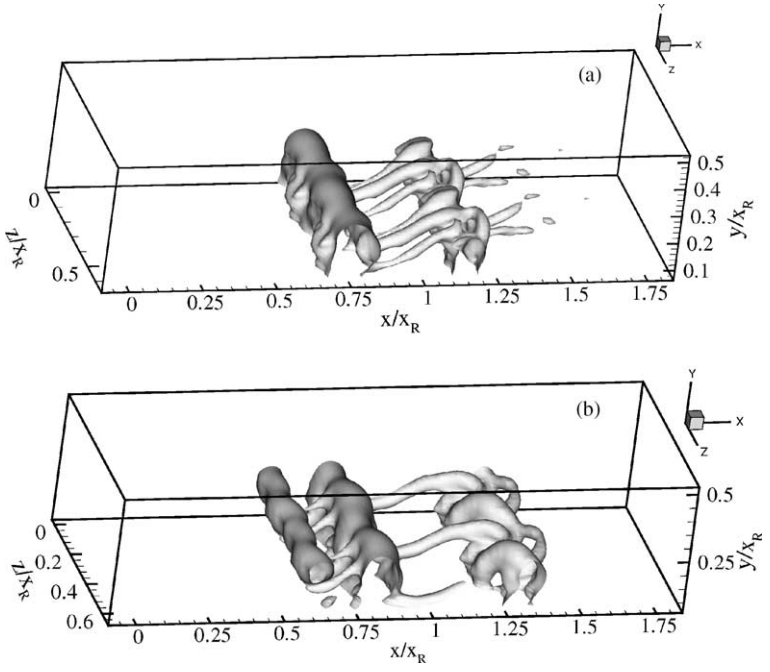

Fig. 11. Low-pressure isosurfaces displaying how *Kelvin–Helmholtz* rolls have been transformed into longitudinal *Ribs* vortices: (a) $t = 305.4D/U_0$; (b) $t = 333.6D/U_0$.

merging and vortex amalgamation take place. In both figures, and for almost all the velocity components and pressure spectra, there is a dominant frequency corresponding to a Strouhal value ranging between $0.225 \leqslant St \leqslant 0.275$. This is the characteristic frequency corresponding to the shedding of large-scale structures from the reattaching shear layer. The spectra for both the velocity components and pressure spectra show some amplified modes between $0.1 \leqslant St \leqslant 0.2$. The U and W velocity spectra clearly indicate a peak frequency approximately at $St = 0.125$. Both the velocity V and the pressure spectra show an amplified peak frequency at

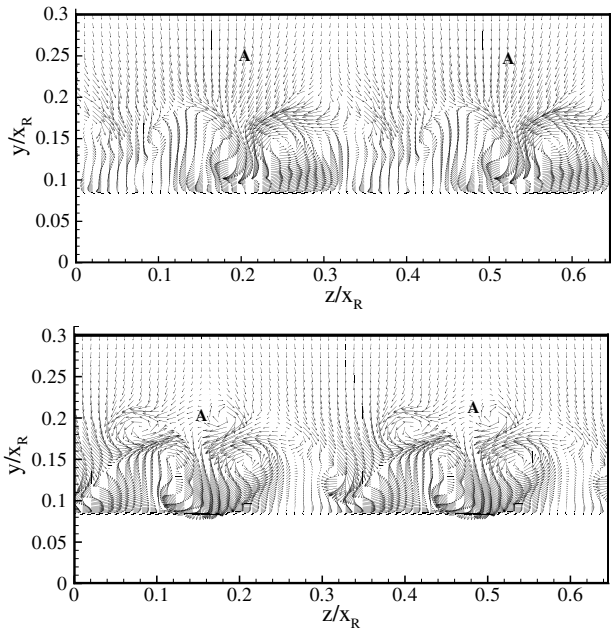

Fig. 12. Velocity vectors (v, w) on the (y, z) plane at the streamwise location $x/x_r = 0.8$.

about $St = 0.175$. A possible explanation for frequency contents in the range of $0.1 \leqslant St \leqslant 0.2$ could be associated with the pairing of vortices to form larger counterparts. For a backward-facing step, Delcayre (1997) evaluated the frequency of pairing to be of order $St = 0.12$.

Thus the mechanism responsible for development and evolution of these streamwise vortical structures in the case of a blunt plate could be similar to that reported by Delcayre (1997) for a backward facing step, the "helical-pairing" instability.

5. Conclusion

The transitional flow over a blunt plate held normal to a uniform stream has been simulated numerically. The LES results compare reasonably well with the available experimental data. The transition process to turbulence has been elucidated and visualised. From detailed analysis of the LES data it has been shown that transition starts with the 2D instability of the free shear layer formed in the separation bubble which is inviscidly unstable via the *Kelvin–Helmholtz* instability mechanism, and the initial unsteadiness starts in the region from $x/x_R = 0.2$ to $x/x_R = 0.25$. Significant growth of the disturbances start at about $x/x_R = 0.5$ but larger-scale structures still remain fairly organised at this location and further downstream at about $x/x_R = 0.7$ the structures appear to be irregular. Breakdown to turbulence occurs around the mean reattachment point and the spanwise symmetry is totally broken at $x/x_R = 0.95$.

Flow visualisation has shown that different large-scale structures have been observed at various stages of the transition process. The Kelvin–Helmholtz billows have been formed initially downstream of the plate leading edge at the onset of *Kelvin–Helmholtz* instability. The *Kelvin–Helmholtz* rolls grow in size and are subjected to approximately sinusoidal (waviness) along the spanwise while travelling downstream. Further downstream the disturbed *Kelvin–Helmholtz* billows roll up, leading to streamwise vorticity formation, with Λ-shaped and streamwise *ribs* being observed in the region $x/x_R = 0.75$ to $x/x_R = 1.5$. It is evident from the current study that the transformation of the *Kelvin–Helmholtz* rolls into 3D structures is most likely to be due to helical instability associated with helical pairing of vortices.

The pressure and velocity spectra have shown that the vortex shedding from the separated shear layer is not periodic in the sense that a unique frequency exists. There is a dominant frequency corresponding to a Strouhal value ranging between $0.225 \leqslant St \leqslant 0.275$ which is the characteristic frequency corresponding to the shedding of large scale structures from the shear layer. In addition, the velocity and pressure spectra clearly indicate an amplified frequency in the range $0.1 \leqslant St \leqslant 0.2$. A possible explanation for this is the pairing of vortices, confirming that the secondary instability in the present study, as mentioned above, is helical instability associated with helical pairing of vortices.

Acknowledgements

The computations were carried out on Cray T3E at Manchester University, funded by EPSRC under the LES-UK2 Consortium.

References

Abdalla, I.E., Yang, Z., in press. Computational visualisation of separated–reattached transitional flow on a blunt plate. Journal of Flow Visualisation and Image Processing.

Bandyopadhyay, P., 1991. Instabilities and large structures in reattaching boundary layers. AIAA Journal 29, 1149–1155.

Bernal, L.P., Breidenthal, R., Brown, G.L., Konrad, J.H., Roshko, A., 1981. On the development of three-dimensional small scales in turbulent mixing layers. In: Proceedings of the 2nd Symposium on Turbulent Shear Flows, Berlin, pp. 305–313.

Breidenthal, R., 1980. Response of plain shear layers and wakes to strong three-dimensional disturbances. Phys. Fluids 23, 1929–1934.

Browan, G.L., Roshko, A., 1974. On density effects and large structure in turbulent mixing layers. J. Fluid Mech. 64, 775–816.

Browand, F.K., Trout, T.R., 1980. A note on spanwise structure in the two-dimensional mixing layer. J. Fluid Mech. 97, 771–781.

Castro, I.P., Epik, E., 1998. Boundary layer development after a separated region. J. Fluid Mech. 374, 91–116.

Chandrasekhar, S., 1961. Hydrodynamic and Hydromagnetic Stability. Clarendon Press, Oxford.

Chandrsuda, C., Mehta, R.D., Weir, A.D., Bradshaw, P., 1978. Effect of free-stream turbulence on large structure in turbulent mixing layers. J. Fluid Mech. 85, 693–704.

Cherry, N.J., Hillier, R., Latour, M.E.M.P., 1984. Unsteady measurements in a separating and reattaching flow. J. Fluid Mech. 144, 13–46.

Comte, P., Lesieur, M., Lamballaise, E., 1992. Large- and small-scale stirring of vorticity and passive scalar in a three-dimensional temporal mixing layer. Phys. Fluids A. 4, 2761–2778.

Delcayre, F., 1997. Topology of coherent vortices in the reattachment region of a backward-facing step. In: Proceedings of the 11th Symposium on Turbulent Shear Flows, Grenoble, France, 3, pp. 6–24.

Djilali, N., Gartshore, I.S., 1991. Turbulent flow around a bluff rectangular plate. Part I: Experimental Investigation. ASME Journal of Fluids Engineering 113, 51–59.

Hillier, R., Cherry, N.J., 1981. The effect of stream turbulence on separation bubble. J. Wind Engng. Ind. Aerodyn 8, 49–58.

Kiya, M., Sasaki, K., 1983. Structure of a turbulent separation bubble. J. Fluid Mech. 137, 83–113.

Kiya, M., Sasaki, K., 1985. Structure of large-scale vortices and unsteady reverse flow in the reattaching zone of a turbulent separation bubble. J. Fluid Mech. 120, 219–244.

Lasheras, J.C., Choi, H., 1988. Three-dimensional instability of a plane free shear layer: an experimental study of the formation and evolution of streamwise vortices. J. Fluid Mech. 189, 53–86.

Manneville, P., 1990. Dissipative Structures and Week Turbulence. Academic Press, New York.

Miksad, R.W., 1972. Experiments on the non-linear stages of free-shear-layer transition. J. Fluid Mech. 56, 695–719.

Neto, A.S., Grand, D., Metais, O., Lesieur, M., 1993. A numerical investigation of the coherent vortices in turbulence behind a backward-facing step. J. Fluid Mech. 256, 1–25.

Oguchi, H., Inoue, O., 1984. Mixing layer produced by a screen and it is dependence on initial conditions. J. Fluid Mech. 142, 217–231.

Pierrehumbert, R.T., 1986. Universal short-wave instability of two-dimensional eddies in an inviscid fluid. Phys. Rev. Lett. 57, 2157–2159.

Pierrehumbert, R.T., Widnal, S.E., 1982. The two and three-dimensional instabilities of spatially periodic shear layer. J. Fluid Mech. 114, 59–82.

Pronchick, S.W., Kline, S.J., 1983. An Experimental investigation of the structure of a turbulent reattaching flow behind a backward-facing Step. Stanford University Thermosciences Div. Ep. MD-42.

Roshko, A., 1981. The plane mixing layer flow visualisation results and three-dimensional effects. In: Jimenez, J. (Ed.), Intl. Conf. on the Role of Coherent Structures in Modelling Turbulence and Mixing. In: Lecture notes in Physics, 136. Springer.

Sandham, N.D., Reynolds, W.C., 1991. Three-dimensional simulations of large eddies in the compressible mixing layer. J. Fluid Mech. 224, 133–158.

Srba, J., 1996. An Experimental Study of a Separated/Reattached Flow Behind a Backward-facing Step $Re_h = 37,000$. NASA Tech. Memo. 10384.

Stuart, J.T., 1967. On finite amplitude oscillations in laminar mixing layers. J. Fluid Mech. 29, 417–440.

Tafti, D.K., Vanka, S.P., 1991. Numerical study of flow separation and reattachment on a blunt plate. Phys. Fluids A 3 (7), 1749–1759.

Winant, C.D., Browand, F.K., 1974. Vortex pairing: the mechanism of turbulent mixing layer growth at moderate Reynolds number. J. Fluid Mech. 63, 237–255.

Wygnanski, I., Oster, D., Fiedler, H., Dziomba, B., 1979. On the perseverance of a quasi-two-dimensional eddy-structure in a turbulent Mixing Layer. J. Fluid Mech. 93, 325–335.

Yang, Z., Voke, R.P., 2000. Large-eddy simulation of separated leading-edge flow in general co-ordinates. International J. Numer. Meth. Engng. 49, 681–696.

Yang, Z., Voke, R.P., 2001. Large-eddy simulation of boundary-layer separation and transition at a change of surface curvature. J. Fluid Mech. 439, 305–333.